Chiral magnetic domain walls under transverse fields: a semi-analytical model

Pierre Géhanne, Andre Thiaville, Stanislas Rohart, Vincent Jeudy

Chiral magnetic domain walls under transverse fields: a semi-analytical model

Pierre Géhanne, André Thiaville,* Stanislas Rohart, and Vincent Jeudy
Laboratoire de Physique des Solides, Université Paris-Saclay, CNRS UMR 8502, 91405 Orsay, France
(Dated: March 25, 2021)

An analytical model for the domain wall structure in ultrathin films with perpendicular easy axis and interfacial Dzyaloshinskii-Moriya interaction, submitted to an arbitrary in-plane magnetic field, is presented. Its solution is simplified to the numerical minimization of an analytic function of just one variable. The model predictions are compared to numerical micromagnetic simulations, using parameters of existing samples, revealing a very good agreement. Remaining differences are analyzed, and partly corrected. Differences with the predictions of the simplest model, usually found in the literature, in which only the domain wall moment's in-plane orientation can vary, are exemplified. The model allows accurate computations, as a function of in-plane field module and orientation, of the domain wall tension and width, quantities controlling the creep motion of domain walls in such films.

I. INTRODUCTION

The interfacial Dzyaloshinskii-Moriya (DMI) interaction was shown, in the last years, to have an important role on the magnetization statics and dynamics [1], especially in the case of magnetic domain walls. This holds not only for epitaxial atomic monolayers on single-crystal substrates [2, 3], but also for the polycrystalline ultrathin films which are at the heart of present spintronic devices [4]. The interfacial DMI, like the DMI introduced many years ago [5, 6], is allowed only when spatial inversion symmetry is broken. Such symmetry breaking takes place naturally at interfaces [7]. DMI is expressed as an exchange interaction with an anti-symmetric matrix. The form of this matrix is dictated by the symmetry of the atomic arrangement, according to the Moriya rules [6]. Interfacial DMI, in the limiting case of maximal symmetry compatible with the presence of an interface (like for two amorphous materials on each side of the interface), and specializing to a film with perpendicular magnetization, applies to the moments in such domain walls a chiral in-plane effective field. As a consequence, the application of in-plane fields on such samples has become a very common experimental tool to study and control the effect of the interfacial DMI.

As the applied fields can be large (because the DMI-induced effective field can also be), the effect of these fields on the domain wall structure and dynamics should be precisely appreciated. However, the complete recalculation of the one-dimensional domain wall profile under an in-plane field has not been performed systematically (as the DMI was absent in the previous works [8, 9]), and various approximations have been recently considered in the presence of DMI [4, 10–12]. It is the goal of this paper to describe an accurate semi-analytical method to perform such calculations, based on the 'small circle' Ansatz employed by A. Hubert a long time ago [9], as we have found that this model describes rather well the situation. The accuracy of these calculations is indeed required for reliably estimating the domain wall surface tension [13], which is numerically very sensitive as it involves the second derivative of the domain wall energy. The importance of this parameter, different from the domain wall surface energy, for the domain wall motion in the creep regime was realized recently [13]. Moreover, the variations of the domain wall width, which have recently been shown to affect the pinning of domain walls [14], are also obtained by this model.

Along the paper, semi-analytical results are compared to micromagnetic simulations, using as parameters those of several Pt/Co ultrathin films that were studied elsewhere [14]. They are also compared to the simplest model (called 'constrained model' hereafter) in which the domain wall profile is fixed, except for the in-plane angle of the domain wall magnetization [4, 10, 11, 13] (note that less constrained variants exist, for example with a variable domain wall width [12]). After describing generally the small circle model (Sec. II) [15], the case where the in-plane field is applied along the domain-wall normal is first treated, as it is the most considered configuration (Sec. III). Then the general case of a field applied at an arbitrary angle with respect to the domain wall is treated, by the same method (Sec. IV). The obtained solutions are used to evaluate the important parameters of the domain wall, namely its width (several definitions are considered, corresponding to different physical meanings of this width), and energy. In the last section, the domain wall surface tension is also evaluated.

II. SMALL CIRCLE MODEL

The reference frame used throughout is set by x the direction of the applied field, and z the normal to the film. The domain wall normal is the $\vec{n}$ direction, with $\vec{m} = (0, 0, 1)$ representing the unit magnetization vector in the domain for $n < 0$ (n is the abscissa along the $\vec{n}$ direction), far from the wall. In the presence of an in-plane field, magnitude H (positive by construction), the magnetization in the domains rotates from $(0, 0, \pm 1)$ to

* andre.thiaville@universite-paris-saclay.fr

$(h, 0, \pm\sqrt{1-h^2})$. We define $h \equiv H/H_{K0}$ the reduced applied field, $H_{K0} = 2K_0/(\mu_0 M_\mathrm{s})$ being the effective anisotropy field of the sample, with $K_0 = K_u - \mu_0 M_\mathrm{s}^2/2$ the effective anisotropy including the thin film demagnetzing effect for perpendicular magnetization, the uniaxial anisotropy constant K_u itself consisting of bulk crystalline and interface anisotropy. The interfacial DMI in the considered samples favors Néel walls, with a chirality fixed by the sign of the DMI constant. The samples considered for the numerical evaluations are Pt/Co/Pt, Pt/Co/Au and Au/Co/Pt, with a nominal cobalt thickness of 0.9 nm, in which the DMI constant D varies widely.

The 'small circle' Ansatz, is depicted in Fig. 1. Under the influence of the in-plane field, the magnetization in the domains rotates out of the poles to points denoted G and G'. A domain wall is, quite generally, a path on the sphere that connects these two points. The internal magnetostatic energy of the domain wall favors equally the two paths that are parallel to the domain wall orientation, whereas DMI favors only one path orthogonal to the domain wall orientation, and applied field favors also only one path, through point E of Fig. 1(a). The idea of the Ansatz is to simplify the task by looking at paths that are contained within a plane, so moderately long. This restriction allows analytical calculations nearly up to the end, and we will show below that it corresponds well to numerical simulation results. The cut of the unit sphere by a plane gives, by definition, a small circle, hence the name of this Ansatz. The family of planes going through points G and G' is described by a single parameter, the 'cut angle' φ, with $-\pi/2 < \varphi < \pi/2$. The magnetization position on the small circle is described by an angle θ. It increases from θ_0 to $\pi - \theta_0$ for the short path C_+, and decreases from θ_0 to $-\pi - \theta_0$ for the long path C_-. From the drawings, the radius of the small circle is $r = \sqrt{1 - h^2 \sin^2\varphi}$, and the coordinates of the center C are $\overrightarrow{OC} = (h\sin^2\varphi, -h\sin\varphi\cos\varphi, 0)$. Thus, the magnetization along the small circle reads

$$\vec{m} = \begin{pmatrix} h\sin^2\varphi + r\cos\varphi\sin\theta \\ -h\sin\varphi\cos\varphi + r\sin\varphi\sin\theta \\ r\cos\theta \end{pmatrix} \qquad (1)$$

The angle θ_0 along the small circle that corresponds to the domains magnetization satisfies $\sin\theta_0 = h\cos\varphi/r$ and $\cos\theta_0 = \sqrt{1-h^2}/r$. Note that by definition one has $0 < \theta_0 < \pi/2$ and $h > 0$.

III. FIELD NORMAL TO THE DOMAIN WALL

This is a high symmetry situation (the x axis and the n axis coincide), where the applied field H and the DMI-induced effective field at the domain wall are collinear. When these two fields point in the same sense (and their sum is sufficiently large), the solution is the Néel wall of the corresponding chirality. When the applied field is opposite to the DMI field and sufficiently large, the solution is again a Néel wall, with reversed chirality. When the applied field is close to compensate the DMI effective field, an intermediate Bloch-Néel wall may appear.

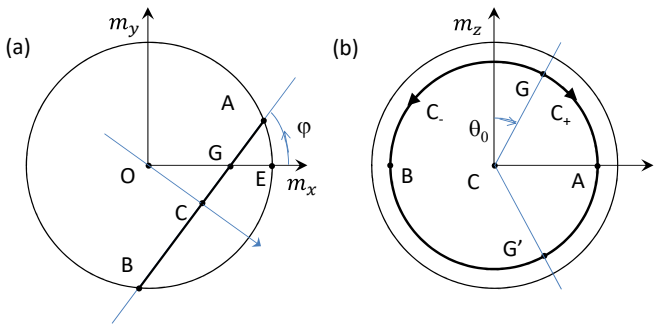

Figure 1. The 'small circle' Ansatz. (a) Top view of the unit sphere for the magnetization vectors, under an in-plane field in the $+x$ direction. Point G depicts the magnetization orientation in the $n < 0$ domain (and hides point G' which corresponds to the $n > 0$ domain). A small circle of the unit sphere, that goes through G and G' and is vertical, is defined by the cut angle φ, which has to be optimized for each situation. Point C is the center of this small circle. The in-plane angle of the domain wall magnetization, called ψ, is defined by the angle of OA with OE; it is thus different from φ. (b) Side view in the direction normal to the small circle, showing the two paths that connect G to G', either through A (short path C_+ where θ increases), or through B (long path C_- where θ decreases). The great circle (radius 1) is also drawn in thin line.

A. Semi-analytical model

The densities for the exchange, DMI, effective uniaxial anisotropy, Zeeman and domain wall internal magnetostatic energy are, respectively,

$$\mathcal{E}_\mathrm{exc} = Ar^2\left(\frac{d\theta}{dn}\right)^2, \qquad (2a)$$

$$\mathcal{E}_\mathrm{DMI} = -D\frac{d\theta}{dn}r(h\sin^2\varphi\sin\theta + r\cos\varphi), \qquad (2b)$$

$$\mathcal{E}_\mathrm{anis} = K_0\left(h^2\sin^2\varphi + r^2\sin^2\theta\right), \qquad (2c)$$

$$\mathcal{E}_\mathrm{Z} = -\mu_0 M_\mathrm{s} H\left(h\sin^2\varphi + r\cos\varphi\sin\theta\right), \qquad (2d)$$

$$\mathcal{E}_\mathrm{BN} = K\cos^2\varphi\,(h\cos\varphi - r\sin\theta)^2. \qquad (2e)$$

In the last expression, K is the effective magnetostatic term related to the domain wall, i.e. the magnetostatic cost of a Néel wall. In the ultrathin limit (sample thickness $t \ll$ domain wall width parameter Δ_0 where $\Delta_0 = \sqrt{A/K_0}$), it reads $K \approx \mu_0 M_\mathrm{s}^2 t \ln 2/(2\pi\Delta)$ [16]. The DMI-induced effective field at the domain wall is $H_\mathrm{DMI} = D/(\mu_0 M_\mathrm{s}\Delta_0)$.

The integral of the total energy density $\mathcal{E}$ has to be minimized with respect to the function $\theta(n)$, with the constrains $\theta(-\infty) = \theta_0$, $\theta(+\infty) = \pi - \theta_0$. Inspection

of the terms of Eq. (2) shows that (i) the DMI term is the x derivative of some function, hence will play no role in the profile $\theta(n)$; (ii) the energy density has the usual expression of domain walls, with a gradient squared plus a function of θ. Therefore, the associated first integral can be written, leading to the angle differential variation law

$$\frac{d\theta}{d\xi} = \sqrt{1+\kappa\cos^2\varphi}\,(\sin\theta - \sin\theta_0)\,, \tag{3}$$

where the reduced variables $\xi = n/\Delta_0$ and $\kappa = K/K_0$ have been introduced. This relation can be integrated [8], a surprisingly simple formulation of this result being [9]

$$\sin\theta = \sin\theta_0 + \frac{\cos^2\theta_0}{\sin\theta_0 + \cosh\left(\xi\cos\theta_0\sqrt{1+\kappa\cos^2\varphi}\right)}. \tag{4}$$

From Eq. (3), the energy of the domain wall can be evaluated. It is given by the integral of $\mathcal{E} + K_0 h^2$, the last term having been included to remove the energy density in the domains. Using the condition (3) to simplify the calculations, one obtains finally

$$\frac{\sigma_+}{\sigma_0} = r^2\sqrt{1+\kappa\cos^2\varphi}\left[\cos\theta_0 - \left(\frac{\pi}{2}-\theta_0\right)\sin\theta_0\right] - r\delta\left[h\sin^2\varphi\cos\theta_0 + (\frac{\pi}{2}-\theta_0)r\cos\varphi\right] \tag{5a}$$

$$\frac{\sigma_-}{\sigma_0} = r^2\sqrt{1+\kappa\cos^2\varphi}\left[\cos\theta_0 + \left(\frac{\pi}{2}+\theta_0\right)\sin\theta_0\right] - r\delta\left[h\sin^2\varphi\cos\theta_0 - (\frac{\pi}{2}+\theta_0)r\cos\varphi\right]. \tag{5b}$$

In this expression, $\delta = D/(2\sqrt{AK_0}) = (2/\pi)D/D_c$ is the reduced DMI constant, with $D_c = (4/\pi)\sqrt{AK_0}$ the well-known critical value of DMI [neglecting the Bloch-Néel anisotropy energy of Eq. (2e)] above which the uniform magnetic state is unstable. In the constrained model [4, 10, 11] where only the in-plane angle (called ψ) of the domain wall magnetization can vary, one simply has to minimize versus ψ the expression $\sigma(\psi)/\sigma_0 = 1 + (\kappa/2)\cos^2\psi - (\pi/2)(\delta+h)\cos\psi$.

Let us now look at a few limiting cases. When $H = 0$, the small circle is a great circle so $r = 1$, $\theta_0 = 0$, and the cut angle φ is the angle of the domain wall magnetization ($\varphi = \psi = 0$ for Néel walls, $\pi/2$ for Bloch walls). The domain wall energy simplifies to

$$\frac{\sigma_\pm}{\sigma_0} = \sqrt{1+\kappa\cos^2\varphi} \mp \frac{\pi}{2}\delta\cos\varphi. \tag{6}$$

For $\delta > 0$, the energy minimum is obtained with σ_+, and at $\cos^2\varphi = (\pi\delta/2)^2/\left[\kappa^2 - \kappa(\pi\delta/2)^2\right]$. This value reaches 1 for

$$\delta = \delta_c \equiv \frac{2}{\pi}\frac{\kappa}{\sqrt{1+\kappa}}. \tag{7}$$

This relation is a more general expression of the critical value of the DMI at which the uniform state becomes unstable, as it takes better into account the internal magnetostatic energy of Néel walls. The expression at leading order is $\delta_c = 2\kappa/\pi$ [4]; the practical difference is weak as κ vanishes in the limit of zero thickness (for the samples studied here one indeed has $\kappa \simeq 0.1$).

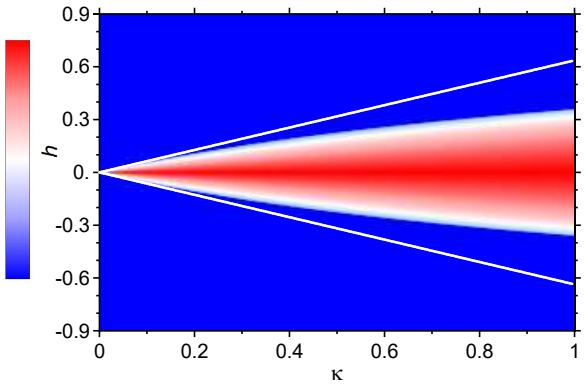

Figure 2. Results of the numerical minimization using the 'small circle' Ansatz, for the case of zero DMI, $\delta = 0$. The color code of the map shows the small circle cut angle φ, it extends from 0 (blue) to $\pi/2$ (red). The two lines (also obtained in the constrained model) depict the linear relation valid at small κ, see text.

Another limit is the a priori simple case with no DMI $\delta = 0$. Inspection of Eqns. 5a - 5b shows that even in that case the minimization over φ is not simple. The numerical solution of the problem is depicted in Fig. 2, as a map of the cut angle φ in the (h, κ) plane. For small domain wall anisotropy κ, the solution agrees with the simple expectation in the case where the rotation of magnetization in the domains, and the deformation of the profile of the polar angle of the magnetization across the domain wall, are neglected, namely $h = \pm(2/\pi)\kappa$ for the field required to reach the Néel wall structure.

This simple case stresses that, even if the small circle model is easy to write down, its full solution is not. Therefore here stops, in general, the analytical work; one has to continue by a numerical minimization with respect to the cut angle φ. It should be noted that, if the minimum is at $\varphi = 0$, then the solution is exact (within the assumption made for evaluating the energies). The corresponding expressions for the domain wall energies were already given in [17, 18].

To illustrate the model outputs, Fig. 3 shows the results for the case $\kappa = 0.3$ and $\delta = \pm 0.1$, with the field acting in the same sense as DMI when $\delta > 0$, whereas at zero field the wall is in an intermediate Bloch-Néel state. The domain wall energies [Fig. 3(a)] mostly decrease with field, and reach 0 at the effective anisotropy field where the domain wall vanishes as the magnetization turns in-plane, parallel to the field. In the case where DMI and applied fields are parallel, the characteristic negative domain wall energy region [17] is obtained. In the anti-parallel case, the domain wall energy reaches a maximum, before decreasing to 0. This maximum is not

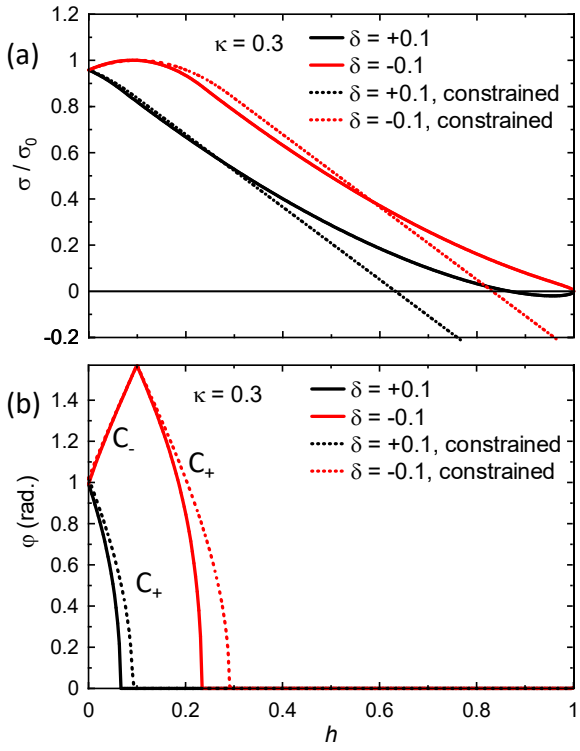

Figure 3. Results of the numerical minimization using the 'small circle' Ansatz, for a large domain wall relative magnetostatic energy ($\kappa = 0.3$), for two opposite and small values of the DMI ($\delta = \pm 0.1$). (a) Normalized domain wall energy. The energy maximum in the antiparallel case occurs at $h \approx 0.0901$. (b) Corresponding cut angle φ, and minimum energy contours $C_\pm$ (see Fig. 1). The value $\varphi = \pi/2$ is reached at $h \approx 0.0995$. The zero-field value $\varphi \approx 1$ radian means that the domain wall is in a mixed Bloch-Néel state with the chosen values of κ and δ. The results of the constrained model are drawn by dotted curves.

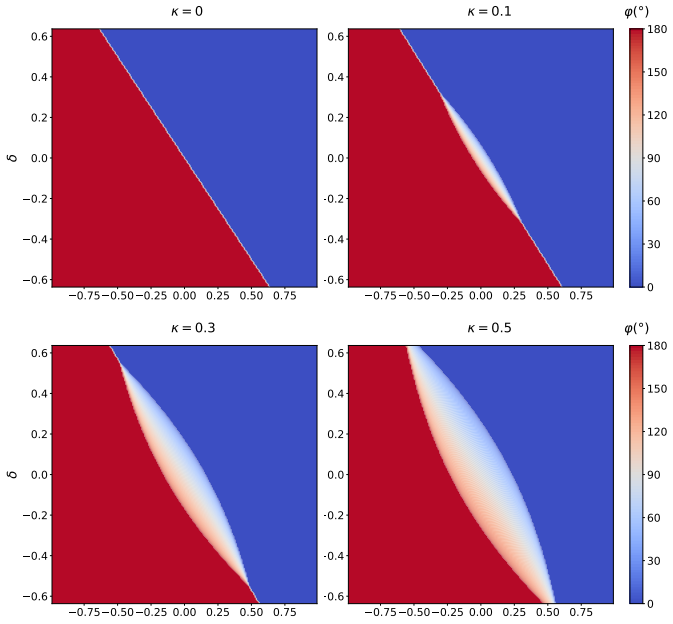

Figure 4. Type of domain wall as a function of in-plane field (scaled field h) and DMI (expressed by the scaled parameter δ), for increasing values of the domain wall magnetostatic energy (scaled parameter κ). For these drawings, a fixed direction in the plane is considered, so that negative fields are figured, and φ spreads over the $[0, \pi]$ interval. The color code represents the cut angle φ, plotted over the extended range from 0 to π so as to differentiate the two chiralities of Néel walls. The constrained model predicts a switching at $h = -\delta$, the ϕ isovalues being parallels to that line.

exactly located at $h = -\delta$ (i.e. $H = -H_{\rm DMI}$), because the domain wall magnetostatic energy is not negligible.

Repeating this calculations for various values of κ, δ and h, phase diagrams can be constructed, as shown in Fig. 4. They illustrate that the switching of the domain wall from one polarity of Néel wall to the other takes place around $h = -\delta/\sqrt{1+\kappa}$, with a mixed Bloch-Néel region that gets larger as κ increases. The above switching field relation can be obtained by equating σ_+ (Eq. 5a) to σ_- (Eq. 5b) under the assumption that $\varphi = 0$ (i.e. Néel walls). The graphs show two switching processes, either continuous and through the Bloch wall in the vicinity of the center of the graphs, or discontinuous from one Néel wall to the opposite one far from the center of the graphs. One can obtain analytically the endpoints of the continuous region as $(h, \delta) = \pm\left(-\sqrt{\kappa/(1+\kappa)}, \sqrt{\kappa}\right)$.

Once the domain wall profile is known, it is possible to compute some quantities of interest. The first one is the so-called Thiele domain wall width $\Delta_{\rm T}$ which governs the domain wall dynamics [19, 20]. It is defined by $2/\Delta_{\rm T} = \int \left(d\vec{m}/dx\right)^2 dx$. One obtains

$$\frac{\Delta_{\rm T}^+}{\Delta_0} = \frac{1}{r^2\sqrt{1+\kappa\cos^2\varphi}\left[\cos\theta_0 - (\frac{\pi}{2}-\theta_0)\sin\theta_0\right]} \quad (8a)$$

$$\frac{\Delta_{\rm T}^-}{\Delta_0} = \frac{1}{r^2\sqrt{1+\kappa\cos^2\varphi}\left[\cos\theta_0 + (\frac{\pi}{2}+\theta_0)\sin\theta_0\right]} \quad (8b)$$

Note that, in the presence of an in-plane field that tilts the magnetization in the domains, the famous steady-state velocity to easy-axis field (H_z) relation becomes

$$v_x = \frac{\gamma_0 \Delta_{\rm T}}{\alpha} H_z \sqrt{1-h^2}, \quad (9)$$

(with $\gamma_0 \equiv \mu_0|\gamma|$ the gyromagnetic factor and α the Gilbert damping parameter, not to be confused with the angle of domain wall normal with field resp. the domain wall tension, both used in Sec. IV). Thus, the velocity increase due to that of the Thiele DW width is partly compensated by the decrease of the driving force due to the domain magnetization tilt, illustrating the fact that the in-plane field has conflicting influences on the domain wall mobility.

The other domain wall width of interest is the 'imaging' width, introduced by A. Hubert [9, 21], which measures the extension in physical space of the domain wall.

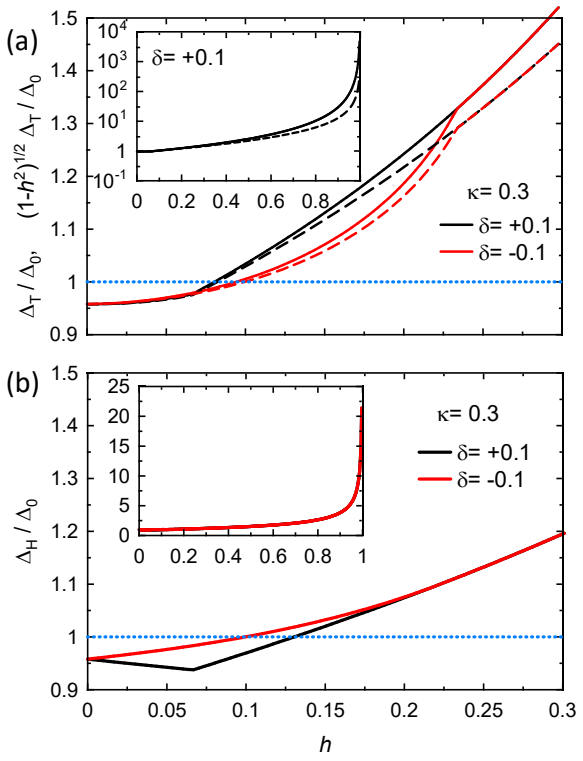

Figure 5. Results of the numerical minimization using the 'small circle' Ansatz, for a large domain wall relative magnetostatic energy ($\kappa = 0.3$), for two opposite and small values of the DMI ($\delta = \pm 0.1$). (a) Thiele domain wall width $\Delta_{\rm T}$ normalized to Δ_0, for the small fields. The inset shows the full curve, in log-lin scale. The dashed curves plot the product $\sqrt{1-h^2}\Delta_{\rm T}$, the relevant quantity for the domain wall mobility. (b) Hubert domain wall width $\Delta_{\rm H}$, normalized to Δ_0, the inset showing the full curve, this time in lin-lin scale. The breaks of the curves correspond to the fields ($h = 0.0664$ for $\delta = +0.1$ and $h = 0.2334$ for $\delta = -0.1$) where the domain wall becomes of the Néel type, perfectly parallel to the field [$\varphi = 0$, see Fig. 3(b)]. The constrained model assumes that all widths are constant, equal to Δ_0 (dotted lines).

It is anticipated that this width is the relevant one to evaluate the pinning of the domain wall by imperfections [14]. Using the general definition of Ref. [21], based on the value of m_z at infinity, one gets

$$\frac{\Delta_{\rm H}^{+}}{\Delta_0} = \frac{\cos\theta_0}{\sqrt{1+\kappa\cos^2\varphi}\,[1-\sin\theta_0]} \qquad (10a)$$

$$\frac{\Delta_{\rm H}^{-}}{\Delta_0} = \frac{\cos\theta_0}{\sqrt{1+\kappa\cos^2\varphi}\,[1+\sin\theta_0]} \qquad (10b)$$

These two widths are plotted in Fig. 5; they globally increase with the in-plane field, as expected. The width smaller than Δ_0 at zero field expresses the contraction due to the magnetostatic cost of the non fully Bloch wall. Whereas the Thiele domain wall width diverges at $H = H_{K0}$ (as no magnetization gradient anymore exists at that field), the Hubert width increases less. In the intermediate field region (intermediate Bloch- state), the width differs for fields parallel and antiparallel to the DMI field. Moreover, in the case of large domain wall anisotropy and low DMI, the Thiele and Hubert widths can show opposite trends with field [Fig. 5(b)]. This is due to the behavior of the various factors entering the domain wall widths, see Eqs. (8,10). Especially, the DW width can decrease with field when the factor containing the DW anisotropy (parameter κ) is dominant, the DW magnetization turning from Bloch to Néel as field increases.

Table I. Parameters of the three samples investigated, all with a nominal 0.9 nm Co thickness (the name reflects the growth order). The exchange constant is assumed to be $A = 16$ pJ/m.

Sample		Au/Co/Pt	Pt/Co/Au	Pt/Co/Pt
$M_{\rm s}$	(kA/m)	1610	1650	1621
K_u	(MJ/m^3)	2.36	2.35	2.12
D	(mJ/m^2)	0.60	-0.87	0
$\mu_0 H_{K0}$	(T)	0.9	0.77	0.58
Δ_0	(nm)	4.7	5.0	5.8
κ	()	0.10	0.11	0.12
δ	()	0.09	-0.20	0

Note also that, for this relatively small DMI compared to the domain wall internal magnetostatic energy, no minimum of the DW width occurs at $H_x = -H_{\rm DMI}$, in contrast with what is predicted by simplified models. Thus, the small circle Ansatz allows an exploration of the complex physics of the statics of domain walls submitted to a transverse field, in which several effects are in competition.

B. Comparison to numerical micromagnetics

We now compare quantitatively the results of the model to those obtained by numerical micromagnetic calculations, using MuMax3 [22]. For these calculations, the sample was meshed in $1024 \times 1 \times 1$ cells in the x, y resp. z directions, with a cell size $1 \times 1 \times 0.9$ nm^3 and periodic boundary conditions in the y direction, the magnetostatic interaction coefficients being summed over 100 000 repetitions (this value was reached by comparison with the analytical demagnetizing factor, for a uniform magnetization). To avoid edge effects, known to exist with DMI [23], the data for the domain wall were collected on the 400 central cells, this length being also well above the obtained domain wall widths. The magnetic parameters of the three samples considered in these calculations are provided in Tab. I (see ref. [14] for details). Important parameters derived from these values are also given, in particular the numbers κ and δ.

The profiles of the domain wall magnetization projected on the (m_x, m_y) plane (this plane was used to draw Fig. 1a) are shown in Fig. 6 (a), as obtained by the small

circle model (dashes), and by numerical micromagnetics (continuous curves), for several values of the in-plane field that span reversal of the domain wall magnetic moment. One first notes that the small circle approximation is very good, as the numerical profiles are extremely close to straight lines, the traces on the (m_x, m_y) plane of the vertical cut plane. Small deviations to this behavior are seen close to the origin of the plots, i.e. at the tails of the domain wall [see Fig. 6(b)]. However, the cut angles are found to differ. This is due to the model's assumption of a purely local z-component of the demagnetizing field, namely $H_{d,z} = -M_s m_z$. Plot (c) shows that indeed the demagnetizing field perpendicular component falls below the -1 ratio to the normal magnetization component m_z, at the domain wall. As a result, the Thiele domain wall width in zero applied field, estimated to be 4.7 nm in the model, is 4.37 nm in the numerical calculation. This leads to a larger demagnetizing cost of the Néel wall, so that the reversal of the domain wall x magnetic moment extends over a larger field region.

Next we look at the energy of the domain wall, per unit surface [24]. As visible in Fig. 7, the small circle model gives precisely the same trend as the numerical simulation, but lower values due to the neglect of the non-local magnetostatic term within the domain wall. A calculation detailed in the Appendix leads to a correction term, dependent on the width of the domain wall, which corrects most of this difference (see Fig. 7).

Finally the widths of the domain wall, either relevant for dynamics (the Thiele domain wall width parameter Δ_T) or for imaging (the Hubert domain wall width parameter Δ_H) are investigated. The comparison of the numerical micromagnetic simulation results with those of the small circle model is detailed in Fig. 8. One sees that, generally, the widths are larger with the small circle model, due to the local approximation for the z component of the demagnetizing field, as well as for the x component [Eq. (2e)]. The computed variations of the domain wall width are important in relative terms. Even if it changes, in absolute terms, only between 4 and 6 nm, an effect on the domain wall pinning characteristics has been experimentally observed [14].

One notices that the widths, in this case where DMI is comparable to or even larger than the domain wall internal magnetostatic energy, show a minimum for some field opposite to the DMI field. This field is however smaller, in absolute value, than the field where the domain wall energy is maximum. Therefore, the various methods based on domain walls to measure the interfacial DMI should be compared in detail.

Globally, the small circle model is shown to be quite accurate, for the magnetization profile, its spatial extent and its energy. The biggest difference appears to lie in the domain wall energy. Most of it may be corrected by adding an estimate of the non-local magnetostatic energy of the domain wall.

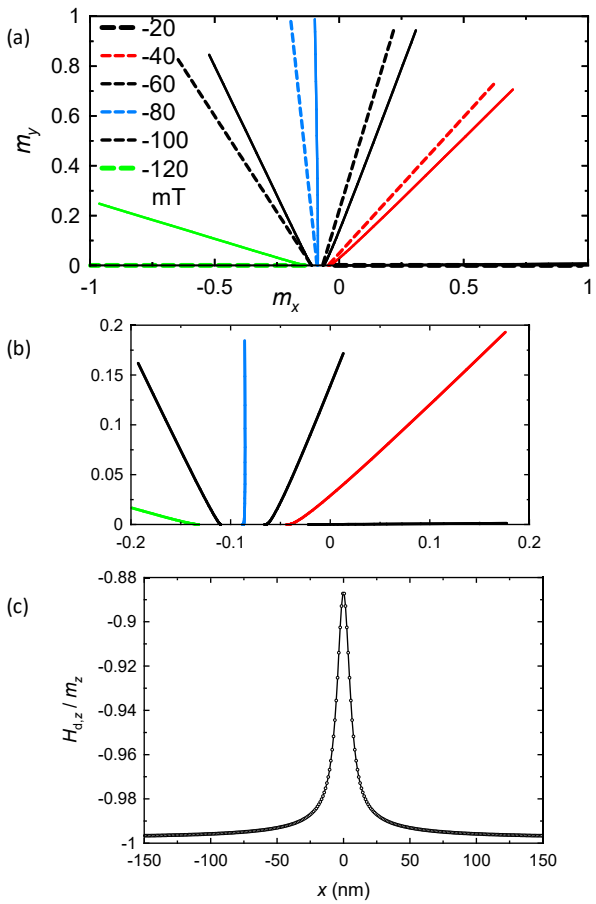

Figure 6. Comparison of the small circle model with numerical simulations, for the Au/Co/Pt sample. (a) The in-plane magnetization components for an up-down domain wall under several in-plane fields, predicted by the small circle model (dashed lines) and computed by numerical micromagnetics (curves). (b) Zoom close to the origin, for the numerical profiles, to evidence the small deviations from linearity. (c) Profile of the local z demagnetizing factor as extracted from the micromagnetic calculation under zero applied field.

IV. FIELD AT AN ARBITRARY ANGLE

For this general case, we proceed similarly to the previous part. Only what changes or was not present in the high symmetry case is given.

A. Semi-analytical model

The angle of the domain wall normal $\vec{n}$ with the field (x) axis is called α. The energy densities which depend on the domain wall orientation are the DMI and domain wall internal magnetostatic energies. They read

$$\begin{aligned}\mathcal{E}_{\rm DMI} &= -D\frac{d\theta}{dn} r\left[h\sin\varphi\sin(\varphi-\alpha)\sin\theta + r\cos(\varphi-\alpha)\right]\\ \mathcal{E}_{\rm BN} &= K\cos^2(\varphi-\alpha)\left(h\cos\varphi - r\sin\theta\right)^2 .\end{aligned} \tag{11}$$

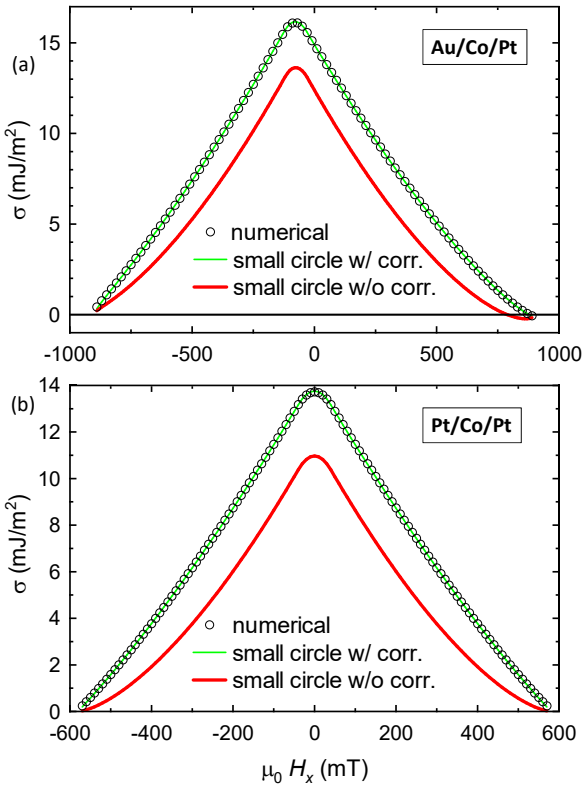

Figure 7. Comparison of the small circle model with numerical simulations, for the Au/Co/Pt (a) and Pt/Co/Pt (b) samples, regarding the domain wall energy. The effect of the analytical domain wall energy correction (see Appendix) is shown. For Au/Co/Pt, the domain wall energy maximum is reached at $\mu_0 H_x = -75$ mT.

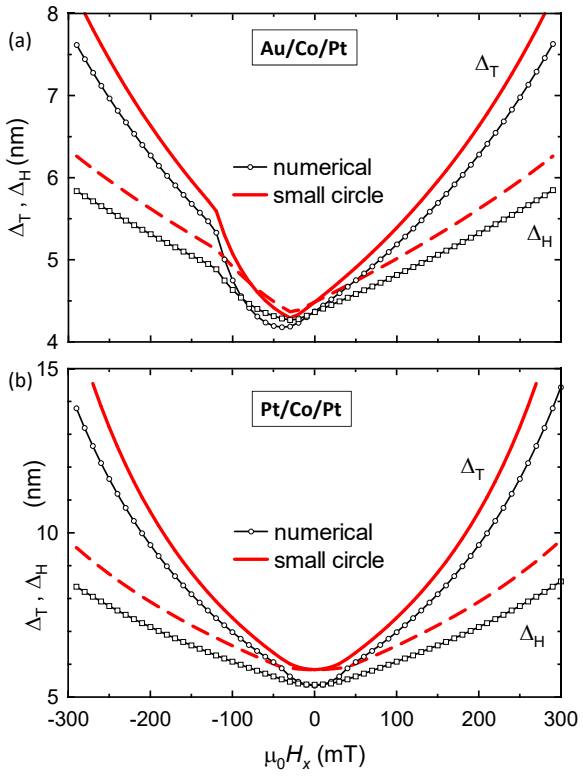

Figure 8. Comparison of the small circle model with numerical simulations, for the AuCoPt (a) and PtCoPt (b) samples, regarding the domain wall widths (see text for definitions). For AuCoPt, all widths show a minimum at -30 mT for the small circle model, and -40 mT for the numerical calculation, values which are clearly lower from that where the domain wall energy is maximum [see Fig. 7(a)].

The same analysis as before leads to the variation law of the angle θ

$$\frac{d\theta}{d\xi} = \sqrt{1+\kappa\cos^2(\varphi-\alpha)}\,(\sin\theta - \sin\theta_0)\,. \qquad (12)$$

Similarly, the domain wall energies for both arcs are

$$\frac{\sigma_+}{\sigma_0} = r^2\sqrt{1+\kappa\cos^2(\varphi-\alpha)}\left[\cos\theta_0 - (\frac{\pi}{2}-\theta_0)\sin\theta_0\right] - r\delta\left[h\sin\varphi\sin(\varphi-\alpha)\cos\theta_0 + (\frac{\pi}{2}-\theta_0)r\cos(\varphi-\alpha)\right], \qquad (13a)$$

$$\frac{\sigma_-}{\sigma_0} = r^2\sqrt{1+\kappa\cos^2(\varphi-\alpha)}\left[\cos\theta_0 + (\frac{\pi}{2}+\theta_0)\sin\theta_0\right] - r\delta\left[h\sin\varphi\sin(\varphi-\alpha)\cos\theta_0 - (\frac{\pi}{2}+\theta_0)r\cos(\varphi-\alpha)\right]. \qquad (13b)$$

Finally, the domain wall widths have similar expressions to the normal case [Eqs. (8, 10)], only replacing φ by $\varphi-\alpha$ inside the square root with κ. These formulas illustrate the power of the model: treating a much more general problem is realized by a minor modification of the functions to use. For the constrained model, counting the domain wall magnetization angle ψ from the domain wall normal, the function to minimize, for each value of α, reads now $\sigma(\psi)/\sigma_0 = 1+(\kappa/2)\cos^2\psi-(\pi/2)[\delta\cos\psi+h\cos(\psi-\alpha)]$.

The computed dependence of the domain wall energy on the domain wall orientation α allows evaluating another important parameter, the domain wall surface tension γ. It is defined by

$$\gamma(\alpha) = \sigma(\alpha) + \frac{d^2\sigma}{d\alpha^2}. \qquad (14)$$

Indeed, in the case of a domain wall surface energy that depends on the domain wall orientation, the energy cost of a bulging of the domain wall consists of (i) the increase of the wall length, penalized by σ, and (ii) an energy variation due to the exploration of neighboring domain wall angles by the bulge, which leads to the second derivative. The distinction between energy and tension is a well-known concept in surface physics [25], and its relevance for magnetic domain wall creep motion was recently stressed [13, 26].

For the demonstration sample with large domain wall internal magnetostatic energy ($\kappa = 0.3$) first, the varia-

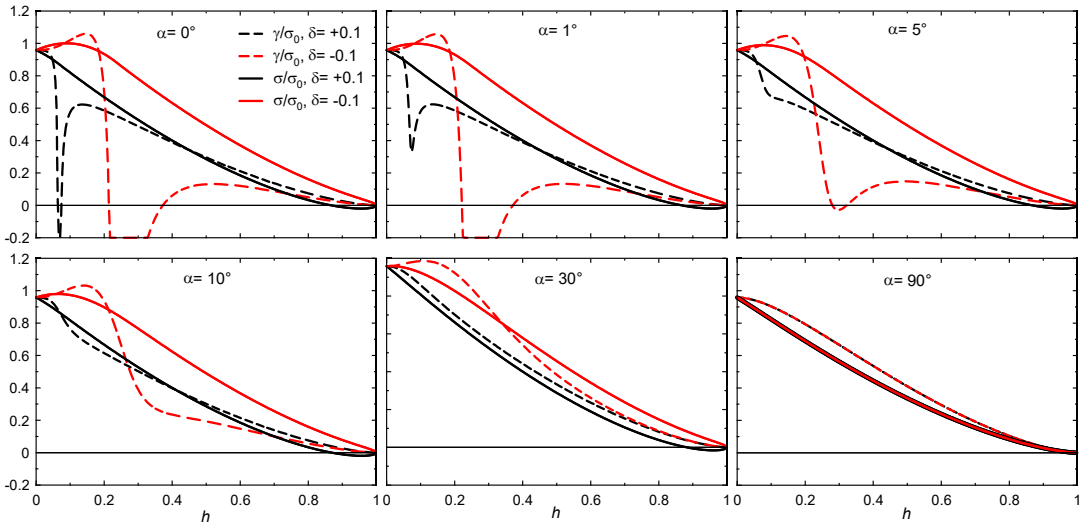

Figure 9. Results of the numerical minimization using the 'small circle' Ansatz, for a large domain wall relative magnetostatic energy ($\kappa = 0.3$), for two opposite and small values of the DMI ($\delta = \pm 0.1$). The domain wall surface energy σ (lines) as well as surface tension γ (dash lines), normalized to the Bloch wall surface energy σ_0, are plotted as a function of the normalized in-plane field h, for several values of the angle α between the domain wall normal and the applied field.

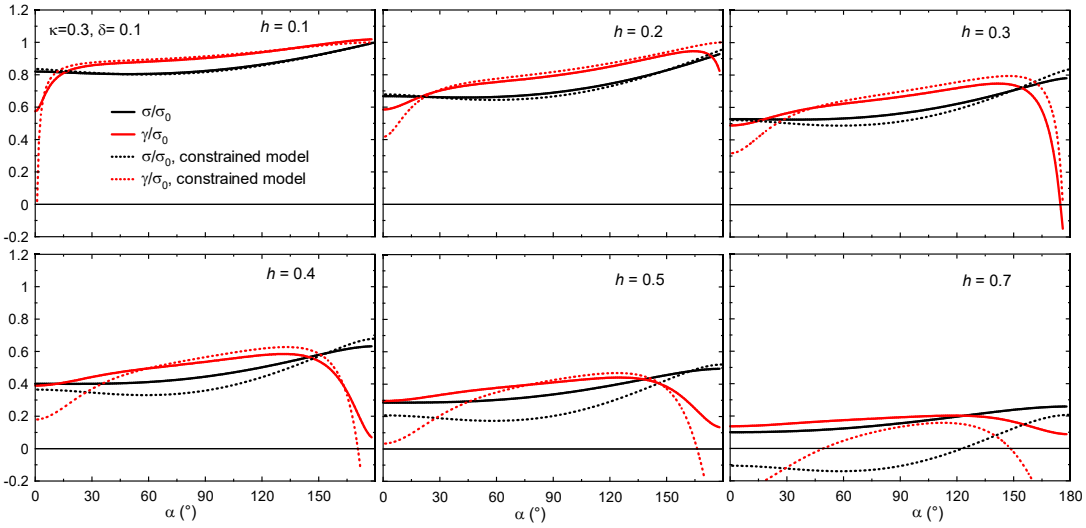

Figure 10. Alternative view of the results shown in Fig. 9, for $\kappa = +0.3$ and $\delta = +0.1$, where the angle α of the domain wall normal with the in-plane field is varied, for selected values of the field. The results of the constrained model have been included (dotted curves) for comparison.

tion of domain wall surface energy and tension as a function of in-plane field and domain wall orientation is shown in Fig. 9. For large angles ($\alpha > 20°$), domain wall energy and tension follow similar evolutions with applied field. One should nevertheless note that the negative domain wall energies found close to saturation give positive tensions. At low angles however, things are much more complex, with the appearance of regions in the (α, h) space where the domain wall tension is negative. This situation is well known in crystal growth [25]: such a domain wall orientation is unstable, and faceting appears (a phenomenon also called the zig-zag faceting in magnetism [9]). The faceting in the case where in-plane field is parallel to DMI field ($\delta > 0$ here) is minute, as the domain wall tension is already postive at $\alpha = 1°$ [for $h = 0.07$ for example, the tension reaches 0 at $\alpha \equiv \alpha_c = 0.515°$ and the faceting occurs with angles (+ or −) $\alpha_f = 1.29°$]. It is larger in the antiparallel case: at $h = 0.3$ the angles

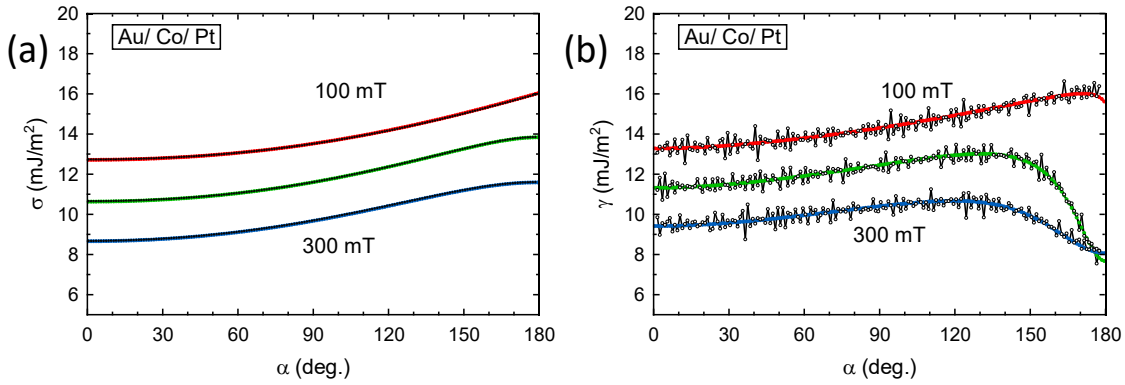

Figure 11. Comparison of the numerical micromagnetics results (open black symbols) to those of the semi-analytical small circle model (colored curves), for the Au/Co/Pt sample. (a) variation of the domain wall energy σ with angle of the applied in-plane field, for 3 values of the field $\mu_0 H = 100, 200, 300$ mT. (b) variation of the domain wall tension γ in the same conditions. The analytical correction to the domain wall energy (and tension) is included in the small circle values. Note the absence of noise in the semi-analytical calculation of the tension, compared to the numerical procedure (see text for cause).

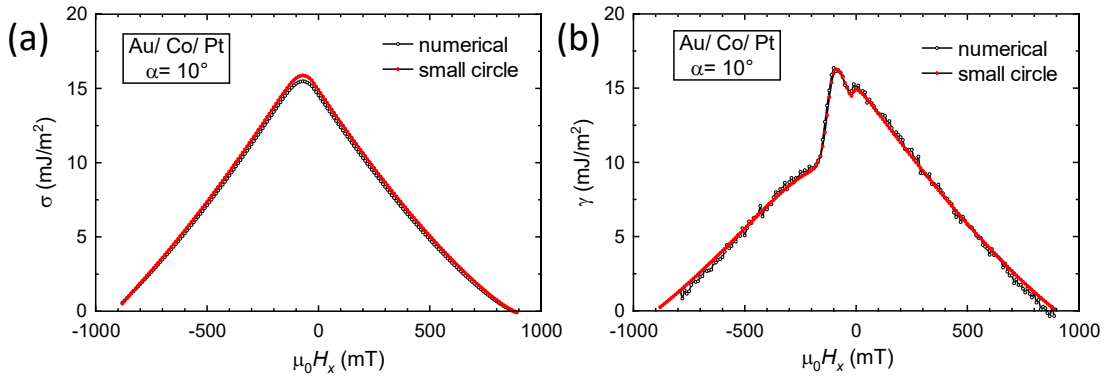

Figure 12. Comparison of the numerical micromagnetics results (open black symbols) to those of the semi-analytical small circle model (red curves), for the Au/Co/Pt sample. (a) variation of the domain wall energy σ with the in-plane field, applied at an angle $\alpha = 10$ degrees. (b) variation of the domain wall tension γ in the same conditions. The analytical correction to the domain wall energy (and tension) is included in the small circle values.

are 5.25° and ±11.3°, respectively. In the $\gamma < 0$ region (i.e. $|\alpha| < \alpha_c$), the domain wall energy σ is replaced by $\sigma_f(\alpha) = \sigma(\alpha_f)\cos\alpha/\cos\alpha_f$, with a discontinuity at $\alpha = \alpha_c$. This relation moreover leads to a domain wall tension which is exactly zero. These conclusions hold, however, only in the infinite domain wall length limit, as the energy cost of the kinks of the faceted domain wall is not taken into account.

Another noticeable feature is that, for moderate angles ($|\alpha| < 20°$), at non-negligible fields ($h > 0.25$) the favored domain wall has a lower energy, but a larger tension.

The other way to look at the same data, in which the angle α varies continuously, is shown in Fig. 10. In addition, the results of the constrained model have been included in these graphs (dashed curves). The differences with the small circle model steadily increase as the field becomes larger, and they are more important for the domain wall tension γ, with larger variations with angle predicted by the constrained model. This should be expected, from the presence of the second derivative of the domain wall energy versus angle, which is sensitive to the fine variations of the domain wall energy σ. The large differences of computed domain wall tension mean large differences of the domain wall mobility as a function of field orientation, hence for example big differences of shape of bubble domains when expanding in the creep regime in the presence of an in-plane field [13].

B. Comparison with numerical micromagnetics

We now turn to the samples investigated in this study. Using the same procedure, the domain wall surface energy σ was numerically evaluated. In order to obtain the domain wall tension γ, a finite differences evaluation of the second derivative versus angle was performed. Due to the limited precision of the numerical values (single precision), the angle step could not be reduced below 1 degree. For the small circle calculations, a much smaller angle step could be used (10^{-5} degree), as the calculations are performed with double precision, resulting into a smaller numerical noise. The analytical correction of the domain wall energy (see Appendix) was added to the small circle model results, using for the domain wall width parameter the Hubert value. As the variation with angle of the Hubert domain wall width is small (for example, ± 0.1 nm around 5.7 nm for Au/Co/Pt at 200 mT), this correction amounts to the same offset for σ and γ.

The comparison of the two models, for the case of the Au/Co/Pt sample, is shown in Fig. 11. The quantitative agreement is close to perfect. The two quantities σ and γ show a strikingly different behavior, even if the applied fields are all above the DMI field: whereas the energy σ monotonously varies with angle, by a small amount, and monotonously decreases as more field is applied, the tension γ shows a marked decrease at intermediate fields, around the antiparallel orientation of the applied field with respect to the DMI field. This difference comes from the strong sensitivity of γ to the $\sigma(\alpha)$ variation. Note for example that, if $\sigma = A\cos\alpha$ then $\gamma = 0$.

In order to see better the difference between domain wall tension and energy, the alternative plot where field is varied, for given values of the angle, is shown in Fig. 12.

Now that the quantitative accuracy of the small circle Ansatz has been demonstrated, the model can be used to obtain detailed predictions. As an example, Fig. 13 shows the computed color-coded maps of the domain wall surface energy σ and tension γ, for the case of the Au/Co/Pt sample. Whereas the σ-map (a) shows the expected larger energy when field is antiparallel to the DMI field (here, at $\alpha = 180°$), the γ-map (b) shows an energy reduction around that orientation, that depends strongly on the applied field. The cut at $\alpha = 180°$ (c) compares the variation of domain wall surface tension with that of the cut angle φ of the small circle, revealing that the deep troughs of γ occur when the domain wall magnetization reorients out of the Néel state. The corresponding maps (not shown) for the symmetrical Pt/Co/Pt sample only show troughs in γ at $\alpha \approx 0, 180, 360°$ and $\mu_0 H \approx 26$ mT.

From these energy maps, maps of energy differences can be constructed, by comparing for the same angle the results for positive and negative fields. These are shown in Fig. 14, for the surface energy and for the surface tension. For Au/Co/Pt which has a positive DMI, and as up-down walls are considered, one expects that $\sigma(H) < \sigma(-H)$ for positive fields. This is indeed obtained [Fig. 14(a)]. However, and as remarked for the large domain wall anisotropy sample, the domain wall tension difference changes sign twice as field is increased [Fig. 14(b)]. Therefore, if domain wall tension γ alone were determining the domain wall velocity, one would expect that the asymmetry of a circular-shape domain expanding in the presence of an in-plane field would reverse twice, giving a sign in accord with that of the energy difference only at intermediate fields. This directly relates to experimental observations [18, 27], as qualita-

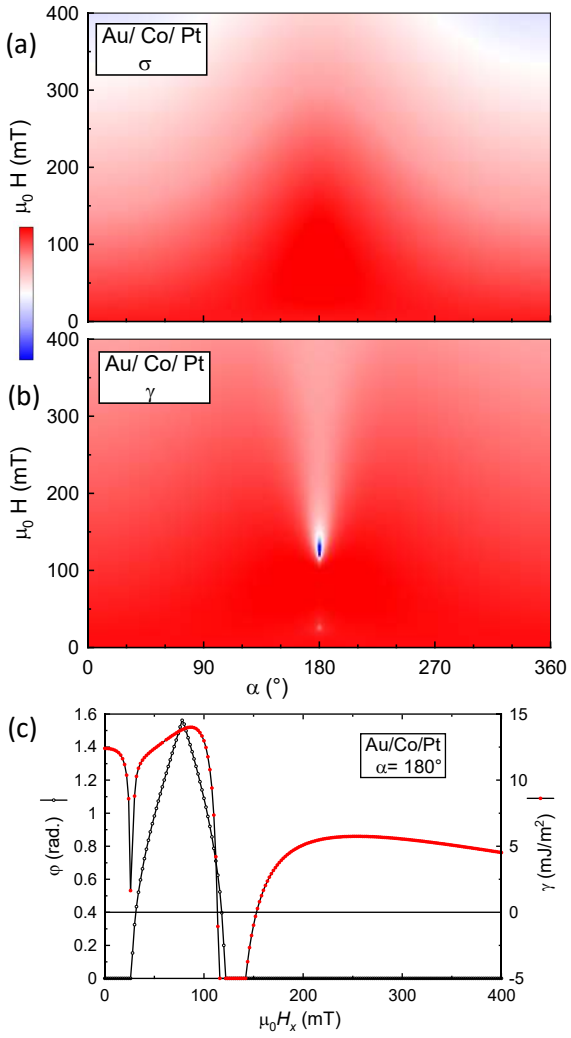

Figure 13. Computed domain wall surface energy σ (a) and tension γ (b) for the Au/Co/Pt sample, by the small circle model incorporating the additional demagnetizing energy. Note that such noiseless maps, containing 360x200 pixels, would have required very long numerical micromagnetics calculation times, whereas a few seconds suffice to produce them using the small circle model, including the magnetostatic correction. The color scale spans the values 0 to +14 mJ/m^2 for (a), and -14 to +14 mJ/m^2 for (b), values outside of these boundaries having been clipped. Panel (c) compares a cut of (b) through $\alpha = 180°$ to the variation of the small circle cut angle φ.

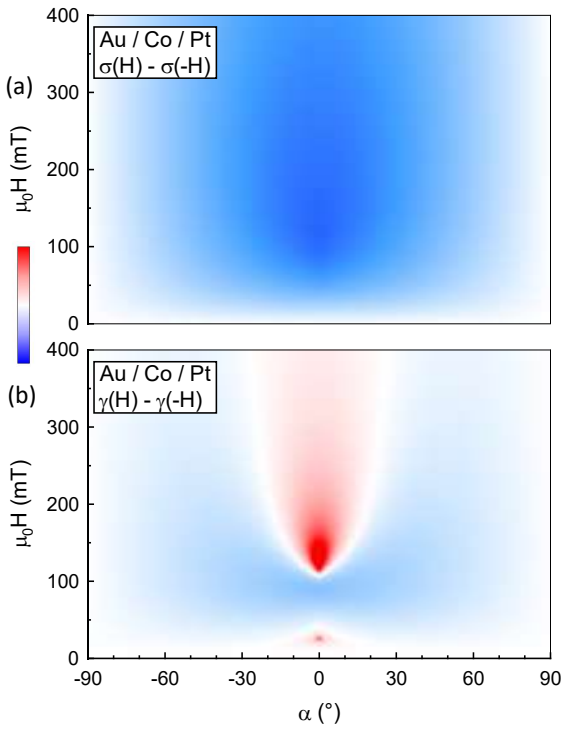

Figure 14. Computed differences of domain wall surface energy σ (a) and tension γ (b) for the Au/Co/Pt sample, between positive and negative fields $\epsilon(\alpha, H) - \epsilon(\alpha, -H)$. The maps are derived from the data of Fig. 13. The color scale spans values -5 to +5 mJ/m^2 for (a), and -10 to +10 mJ/m^2 for (b), values outside of these boundaries having been clipped.

tively explained earlier [13].

V. CONCLUSION

We have developped a semi-analytical model for the one-dimensional domain wall structure in ultrathin films with perpendicular magnetization, in the presence of arbitrary in-plane fields, in orientation and magnitude. The model is based on the 'small circle' Ansatz introduced by A. Hubert. It is semi-analytical, as an analytic expression needs to be minimized versus one variable, the 'cut angle' of the small circle.

The model has been compared to the simplest model of the situation, in which only the orientation of the domain wall magnetic moment is allowed to vary. Clear differences have been observed, that increase as the in-plane field becomes larger. The model ouputs have also been compared to numerical micromagnetic calculations, for three samples having the Au/Co/Pt generic structure, the parameters of which coming from experiments. A very good quantitative agreement has been obtained, with some systematic differences having been uncovered, linked to the magnetostatic energy. A correction to the domain wall energy has been worked out, which leads to much closer values. For the domain wall width however, this is not generally possible as the model computes the full structure of the domain wall.

The model provides the energy and the complete profile of the domain wall, which allows computing the various domain wall widths that are relevant for its statics (Hubert domain wall width), or dynamics (Thiele domain wall width), or any other quantity dependent on the domain wall profile. The complete freedom on the in-plane field allows computing the domain wall surface tension, whose key role has been recently uncovered, with no fear from artefacts due to too restricted energy calculation hypotheses. In particular, the occurence of zero tension regions (in the field-angle space) has been confirmed, meaning that the one-dimensional picture breaks down there, and domain wall faceting occurs. To illustrate the power of semi-analytical means, maps of the domain wall properties as a function of the magnitude and angle of the in-plane field are shown.

It is hoped that the refined calculation of the domain wall properties developed in this work will be useful in constructing a domain wall creep theory which fully incorporates the presence of the in-plane field (a first step being Ref. [26]), quantitatively explaining the surprising results of some experiments [18, 27, 28]. The extension of this methodology to the fast domain wall dynamics should also be investigated.

VI. ACKNOWLEDGEMENTS

This work was supported by Agence Nationale de la Recherche, projects ANR-14-CE26-0012 (ULTRASKY) and ANR-17-CE24-0025 (TOPSKY). We thank Jacques Miltat for a critical reading of the text.

VII. APPENDIX A: ANALYTICAL CORRECTION TO THE DOMAIN WALL MAGNETOSTATIC ENERGY

In the limit of a magnetization uniform across the sample thickness (t), which applies to ultrathin films, the demagnetizing energy E_d of a domain wall with a Bloch profile (domain wall width parameter Δ) can be analytically calculated, by going to Fourier space. This energy diverges, but the difference between two values of Δ is finite. One obtains $E_\mathrm{d}(\Delta = 0) - E_\mathrm{d}(\Delta) = (\mu_0 M_\mathrm{s}^2/2) t I\,(\Delta/t)$, where the integral I reads

$$I(p) = \int_0^{+\infty} \frac{1 - e^{-x}}{x} \left[\frac{4}{\pi x^2} - \frac{\pi p^2}{\sinh^2(\pi p x/2)} \right] dx. \quad (15)$$

On the other hand, the assumption of a local demagnetizing field leads to $E_\mathrm{d}(\Delta = 0) - E_\mathrm{d}(\Delta) = (\mu_0 M_\mathrm{s}^2/2)\,(2\Delta)$. Therefore, the small circle domain wall energy σ should be corrected by adding to it the quantity

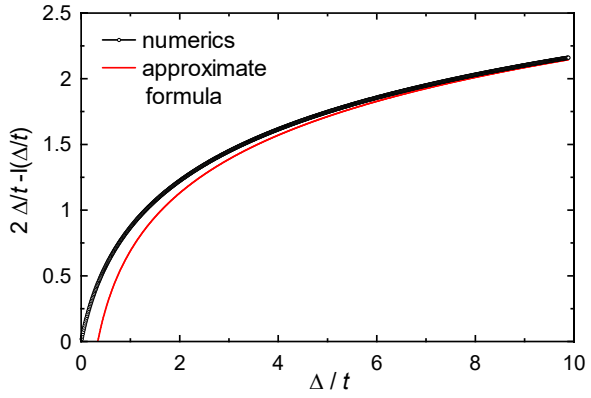

Figure 15. Numerical evaluation of the function giving the demagnetizing energy correction $\sigma_{\rm d}$ to the domain wall energy. The large parameter (i.e. $\Delta \gg t$) asymptotic behavior $0.69 + 0.635\ln(\Delta/t)$ is also drawn.

$\sigma_{\rm d} = (\mu_0 M_{\rm s}^2/2)\,[2\Delta - tI(\Delta/t)]$. The function involved is plotted in Fig. 15. Under an in-plane field, $\sigma_{\rm d}$ should be multiplied by $m_z^2 = (1-h^2)$.

This magnetostatic domain wall energy correction $\sigma_{\rm d}$ can be used to predict the domain wall width more accurately, in the case of zero applied field where the domain wall profile is known. Taking this domain wall width parameter Δ as a variable, one has to minimize the total energy of the domain wall, obtained by integrating the terms of Eq. (2), which reads

$$\sigma(\Delta) = \frac{2A}{\Delta} + 2K_0\Delta + \frac{\mu_0 M_{\rm s}^2}{2} t \left[0.69 + 0.635\ln(\frac{\Delta}{t})\right] \quad (16)$$

(the Bloch-Néel magnetosatic cost, using the first order approximation for the demagnetizing factor of the Néel wall in an ultrathin film [16], is independent of the domain wall width parameter). This results in

$$\Delta = \sqrt{\Delta_0^2 + \left(\frac{0.635t}{4Q_0}\right)^2} - \frac{0.635t}{4Q_0}, \quad (17)$$

where $Q_0 = 2K_0/(\mu_0 M_{\rm s}^2)$ is the quality factor of the sample. As an example, for the Au/Co/Pt sample, one finds $\Delta = 4.385$ nm, much closer to the numerical value. This calculation shows again the origin of the discrepancy between the small circle and the full micromagnetics.

[1] F. Hellman, A. Hoffmann, Y. Tserkovnyak, G. S. D. Beach, E. E. Fullerton, C. Leighton, A. H. MacDonald, D. C. Ralph, D. A. Arena, H. A. Dürr, P. Fischer, J. Grollier, J. P. Heremans, T. Jungwirth, A. V. Kimel, B. Koopmans, I. N. Krivorotov, S. J. May, A. K. Petford-Long, J. M. Rondinelli, N. Samarth, I. K. Schuller, A. N. Slavin, M. D. Stiles, O. Tchernyshyov, A. Thiaville, B. L. Zink, Interface-induced phenomena in magnetism, Rev. Mod. Phys. 89 (2017) 025006.

[2] M. Bode, M. Heide, K. von Bergmann, P. Ferriani, S. Heinze, G. Bihlmayer, A. Kubetzka, O. Pietzsch, S. Blügel, R. Wiesendanger, Chiral magnetic order at surfaces driven by inversion asymmetry, Nature 447 (2007) 190–193.

[3] M. Heide, G. Bihlmayer, S. Blügel, Dzyaloshinskii-moriya interaction accounting for the orientation of magnetic domains in ultrathin films: Fe/w(110), Phys. Rev. B 78 (2008) 140403(R).

[4] A. Thiaville, S. Rohart, É. Jué, V. Cros, A. Fert, Dynamics of Dzyaloshinskii domain walls in ultrathin magnetic films, Europhys. Lett. 100 (2012) 57002.

[5] I. E. Dzialoshinskii, Thermodynamic theory of "weak" ferromagnetism in antiferromagnetic substances, Sov. Phys. JETP 5 (1957) 1259–1272.

[6] T. Moriya, Anisotropic superexchange interaction and weak ferromagnetism, Phys. Rev. 120 (1960) 91–98.

[7] A. Fert, Magnetic and transport properties of metallic multilayers, Materials Science Forum 59-60 (1990) 439–480.

[8] J. Kaczér, R. Gemperle, The rotation of Bloch walls, Czech. J. Phys. 11 (1961) 157–170.

[9] A. Hubert, Theorie der Domänenwände in geordneten Medien, no. 26 in Lecture Notes in Physics, Springer, Berlin, 1974, in german.

[10] S.-G. Je, D.-H. Kim, S.-C. Yoo, B.-C. Min, K.-J. Lee, S.-B. Choe, Asymmetric magnetic domain-wall motion by the Dzyaloshinskii-Moriya interaction, Phys. Rev. B 88 (2013) 214401.

[11] S. Emori, E. Martinez, K.-J. Lee, H.-W. Lee, U. Bauer, S.-M. Ahn, P. Agrawal, D. C. Bono, G. S. D. Beach, Spin Hall torque magnetometry of Dzyaloshinskii domain walls, Phys. Rev. B 90 (2014) 184427.

[12] D.-Y. Kim, D.-H. Kim, S.-B. Choe, Intrinsic asymmetry in chiral domain walls due to the Dzyaloshinskii-Moriya interaction, Appl. Phys. Express 9 (2016) 053001.

[13] J. P. Pellegren, D. Lau, V. Sokalski, dispersive stiffness of Dzyaloshinskii domain walls, Phys. Rev. Lett. 119 (2017) 027203.

[14] P. Géhanne, S. Rohart, A. Thiaville, V. Jeudy, Strength and length scale of the interaction between domain walls and pinning disorder in thin ferromagnetic films, Phys. Rev. Res. 2 (2020) 043134.

[15] The small circle model was already employed in a previous publication by some of us [17], but not described in depth and without incorporating the domain wall internal magnetostatic energy, as it played a minor role in that case.

[16] S. V. Tarasenko, A. Stankiewicz, V. V. Tarasenko, J. Ferré, Bloch wall dynamics in ultrathin ferromagnetic films, J. Magn. Magn. Mater. 189 (1998) 19–24.

[17] S. Pizzini, J. Vogel, S. Rohart, L. D. Buda-Prejbeanu, E. Jué, O. Boulle, I. M. Miron, C. K. Safeer, S. Auffret, G. Gaudin, A. Thiaville, Chirality-induced asymmetric magnetic nucleation in Pt/Co/AlOx ultrathin microstructures, Phys. Rev. Lett. 113 (2014) 047203.

[18] M. Vaňatka, J. C. Rojas-Sánchez, J. Vogel, M. Bonfim,

M. Belmeguenai, Y. Roussigné, A. Stashkevich, A. Thiaville, S. Pizzini, Velocity asymmetry of Dzyaloshinskii domain walls in the creep and flow regimes, J. Phys.: Condens. Matter 27 (2015) 326002.

[19] A. A. Thiele, Applications of the gyrocoupling vector and dissipation dyadic in the dynamics of magnetic domains, J. Appl. Phys. 45 (1974) 377–393.

[20] A. Thiaville, Y. Nakatani, Spin Dynamics in Confined Magnetic Structures III, Springer, Berlin, 2006, Ch. Domain wall dynamics in nanowires and nanostrips, pp. 161–206.

[21] E. Jué, A. Thiaville, S. Pizzini, J. Miltat, J. Sampaio, L. D. Buda-Prejbeanu, S. Rohart, J. Vogel, M. Bonfim, O. Boulle, S. Auffret, I. M. Miron, G. Gaudin, Domain wall dynamics in ultrathin Pt/Co/AlOx microstrips under large combined magnetic fields, Phys. Rev. B 93 (2016) 014403.

[22] A. Vansteenkiste, J. Leliaert, M. Dvornik, M. Helsen, F. Garcia-Sanchez, B. Van Waeyenberge, The design and verification of MuMax3, AIP Adv. 4 (2014) 107133.

[23] S. Rohart, A. Thiaville, Skyrmion confinement in ultrathin film nanostructures in the presence of Dzyaloshinskii-Moriya interaction, Phys. Rev. B 88 (2013) 184422.

[24] For the numerical simulations, three configurations had to be considered: (i) the minimized configuration with a domain wall in the center, (ii) the minimized configuration starting from the all-up state (as well as from the all-down one), (iii) the zero-thickness domain wall configuration, produced by pasting the left half of the all-up to the right half of the all-down minimized configurations. For configuration (iii), no evolution was performed and only the magnetostatic energy was evaluated. The domain wall energy was obtained as $\sigma = L\left[\mathcal{E}(\mathrm{i}) - \mathcal{E}(\mathrm{ii}) + \mathcal{E}_{\mathrm{dem}}(\mathrm{ii}) - \mathcal{E}_{\mathrm{dem}}(\mathrm{iii})\right]$, where L is the width of the central region (400 nm here) and $\mathcal{E}$ resp. $\mathcal{E}_{\mathrm{dem}}$ are total resp. magnetostatic average energy densities computed over that region. The last two terms in the equation allow removing the magnetostatic energy gained when demagnetizing a sample by having it split into two domains. The first difference is necessary because in MuMax3 a uniform configuration magnetized along the easy axis has a large (negative) energy. The domain wall energy is thus obtained by differences from large terms, so that accuracy of these terms is very important.

[25] M. C. Desjonquères, D. Spanjaard, Concepts in Surface Physics, Springer Series in Surface Sciences, vol. 30, Springer, Berlin, 1996.

[26] D. M. F. Hartmann, R. A. Duine, M. J. Meijer, H. J. M. Swagten, R. Lavrijsen, Creep of chiral domain walls, Phys. Rev. B 100 (2019) 094417.

[27] D. Lau, V. Sundar, J.-G. Zhu, V. Sokalski, Energetic molding of chiral magnetic bubbles, Phys. Rev. B 94 (2016) 060401(R).

[28] R. Lavrijsen, D. M. F. Hartmann, A. van den Brink, Y. Yin, B. Barcones, R. A. Duine, M. A. Verheijen, H. J. M. Swagten, B. Koopmans, Asymmetric magnetic bubble expansion under in-plane field in Pt/Co/Pt: effect of interface engineering, Phys. Rev. B 91 (2015) 104414.